

RR LYRAE VARIABLES IN TWO FIELDS IN THE SPHEROID OF M31*

ATA SARAJEDINI¹, CONOR L. MANCONE¹, TOD R. LAUER², ALAN DRESSLER³, WENDY FREEDMAN³, S. C. TRAGER⁴,
CARL GRILLMAIR⁵, AND KENNETH J. MIGHELL²

¹ Department of Astronomy, University of Florida, Gainesville, FL 32611, USA; ata@astro.ufl.edu, cmancone@astro.ufl.edu

² National Optical Astronomy Observatory, P.O. Box 26732, Tucson, AZ 85726, USA; tlauer@noao.edu, kmighell@noao.edu

³ Observatories of the Carnegie Institution of Washington, Pasadena, CA 91101, USA; dressler@ociw.edu, wendy@ociw.edu

⁴ Kapteyn Astronomical Institute, University of Groningen, NL-9700 AV Groningen, Netherlands; scstrager@astro.rug.nl

⁵ Spitzer Science Center, Pasadena, CA 91125, USA; carl@ipac.caltech.edu

Received 2008 October 21; accepted 2009 April 25; published 2009 June 1

ABSTRACT

We present *Hubble Space Telescope* observations taken with the Advanced Camera for Surveys Wide Field Channel of two fields near M32—between 4 and 6 kpc from the center of M31. The data cover a time baseline sufficient for the identification and characterization of 681 RR Lyrae variables of which 555 are ab-type and 126 are c-type. The mean magnitude of these stars is $\langle V \rangle = 25.29 \pm 0.05$, where the uncertainty combines both the random and systematic errors. The location of the stars in the Bailey diagram and the ratio of c-type RR Lyraes to all types are both closer to RR Lyraes in Oosterhoff type I globular clusters in the Milky Way as compared with Oosterhoff II clusters. The mean periods of the ab-type and c-type RR Lyraes are $\langle P_{ab} \rangle = 0.557 \pm 0.003$ and $\langle P_c \rangle = 0.327 \pm 0.003$, respectively, where the uncertainties in each case represent the standard error of the mean. When the periods and amplitudes of the ab-type RR Lyraes in our sample are interpreted in terms of metallicity, we find the metallicity distribution function to be indistinguishable from a Gaussian with a peak at $\langle [\text{Fe}/\text{H}] \rangle = -1.50 \pm 0.02$, where the quoted uncertainty is the standard error of the mean. Using a relation between RR Lyrae luminosity and metallicity along with a reddening of $E(B - V) = 0.08 \pm 0.03$, we find a distance modulus of $(m - M)_0 = 24.46 \pm 0.11$ for M31. We examine the radial metallicity gradient in the environs of M31 using published values for the bulge and halo of M31 as well as the abundances of its dwarf spheroidal companions and globular clusters. In this context, we conclude that the RR Lyraes in our two fields are more likely to be halo objects rather than associated with the bulge or disk of M31, in spite of the fact that they are located at 4–6 kpc in projected distance from the center.

Key words: galaxies: individual (M31) – galaxies: spiral – galaxies: stellar content – stars: variables: other

Online-only material: color figures, figure set, machine-readable and VO tables

1. INTRODUCTION

Pulsating variable stars such as RR Lyraes are powerful probes useful for investigating the properties of stellar populations. The mere presence of RR Lyraes among a population of stars suggests an ancient origin since ages older than ~ 10 Gyr are required to produce RR Lyrae variables. Their periods and amplitudes are a reflection of the metal abundance of the population. Along with their incredible usefulness, RR Lyraes are also relatively straightforward to identify and characterize. This is because of their short periods and the distinct light curve shapes of the ab-types, which pulsate in the fundamental mode and exhibit a relatively rapid rise to maximum and a gradual decline to minimum. This is in contrast to the c-type RR Lyraes which pulsate in the first harmonic and show light curves that are more akin to sine curves. In spite of the great potential RR Lyraes hold as astrophysical tools, they have not been widely studied in our nearest large neighbor galaxy, Andromeda.

One of the first studies attempting to identify RR Lyraes in M31 was that of Pritchett & van den Bergh (1987). They used the Canada–France–Hawaii 3.6 m telescope to observe a field at a distance of 9 kpc from the center of M31 along the minor axis partially overlapping the field observed by Mould & Kristian (1986). They identified 30 RR Lyrae candidates and were able to estimate periods for 28 of them. These ab-type variables have

a mean period of $\langle P_{ab} \rangle = 0.548$ days. The photometric errors in their data prevented them from identifying the lower amplitude c-type RR Lyraes.

The RR Lyrae variables in M31 globular clusters have been investigated by Clementini et al. (2001, cf., Contreras et al. 2008). They used the Wide Field Planetary Camera 2 (WFPC2) onboard the *Hubble Space Telescope* (*HST*) to make the first tentative detection of RR Lyraes in G11, G33, G64, and G322, finding two, four, 11, and eight variables, respectively. Detection and characterization of these stars in globular clusters are more challenging than in the M31 field because of the increased crowding.

Returning to the work on field RR Lyraes, Dolphin et al. (2004) observed the same field as Pritchett & van den Bergh (1987) using the WIYN 3.5 m on Kitt Peak. They found 24 RR Lyrae stars with a completeness fraction of 24%, suggesting that their ~ 100 arcmin² field could contain ~ 100 RR Lyraes resulting in a density of one RR Lyrae per square arcmin. This is much less than the value of ~ 17 arcmin⁻² found by Pritchett & van den Bergh (1987). They also noted for the first time that the mean metallicity of the M31 RR Lyraes seemed to be significantly lower than that of the M31 halo. The work of Durrell et al. (2001) had reported a peak value of $[M/H] \sim -0.8$ for the M31 halo. Dolphin et al. (2004) were not able to reconcile this abundance value with the distance implied by the mean magnitude of their RR Lyrae sample.

The first definitive work on the RR Lyraes of M31 was published by Brown et al. (2004, hereafter B2004) and made use of ~ 84 hr of imaging time (250 exposures over 41 days)

* Based on observations taken with the NASA/ESA *Hubble Space Telescope*, obtained at the Space Telescope Science Telescope.

Table 1
Observing Log

Field	R.A. (J2000)	Decl. (J2000)	Starting Date	Data Sets	Filter	Exp Time	HJD Range (+2 453 000)
1	00 42 41.2	40 46 38	2005 Sep 22	J9H905, J9H906, J9H907, J9H908	F606W	16 × 1136s, 16 × 1177s	635.97 to 638.25
2	00 43 20.8	40 57 25	2006 Feb 9	J9H913, J9H914, J9H915, J9H916	F606W	16 × 1136s, 16 × 1177s	775.88 to 778.96

with the Advanced Camera for Surveys onboard *HST*. Their field was located along the minor axis of M31 approximately 11 kpc from its center. Their analysis revealed a complete sample of RR Lyrae stars consisting of 29 ab-type variables and 25 c-type. The periods of these stars suggest a mean metallicity of $[Fe/H] \sim -1.6$ for the old population in the Andromeda halo. This is qualitatively consistent with the assertions of Dolphin et al. (2004) regarding the metal abundance of the M31 halo—that it is lower than the value suggested by the work of Durrell et al. (2001). More recent work has shown that the M31 halo extends from 30 to 165 kpc (Guhathakurta et al. 2005; Irwin et al. 2005) and has a metallicity that is actually closer to that of the Milky Way halo (Kalirai et al. 2006; Koch et al. 2008).

There is one more paper of note related to this topic and that is the work of Alonso-García et al. (2004). They used the WFPC2 onboard *HST* to image a field ~ 3.5 arcmin to the east of M32 and compared it with a control field that samples the M31 field stars well away from M32. They identify variable stars that they claim are RR Lyraes belonging to M32 therefore suggesting that M32 possesses a population that is older than ~ 10 Gyr. They were not able to classify the RR Lyraes or derive periods and amplitudes for them so their results are not directly comparable to ours.

This review of the literature reveals a significant deficiency in the spatial coverage of RR Lyrae studies in the vicinity of M31. Given the great astrophysical utility of RR Lyrae variables and the expansive size of M31 on the sky, it is clear that a survey of these stars sampling a diversity of regions in Andromeda will provide valuable insights into the star formation and chemical enrichment history of our nearest spiral neighbor.

With this in mind, this paper presents the results of archival *HST* Advanced Camera for Surveys (*HST/ACS*) observations showcasing the RR Lyrae population in the inner regions of the M31 spheroid. The following section describes the observational material and the photometric procedure. We move on to describe the technique used to identify and characterize the variable stars in Section 3. The results of this study are described in Section 4, and a discussion of these results within the broader context of the M31 halo is presented in Section 5. Our conclusions are then summarized in Section 6.

2. OBSERVATIONS

The observations used in the present study were obtained with the *HST/ACS* in parallel with the imagery conducted by program GO-10572. The primary goal of this program was to obtain a deep color–magnitude diagram of the envelope of M32, using the high-resolution channel (HRC) of the ACS. The total envelope exposure was 32 orbits, split between two filters. An identical set of HRC exposures was later obtained in a background field selected to represent the M31 disk+halo contribution to the M32 envelope exposures. The present images

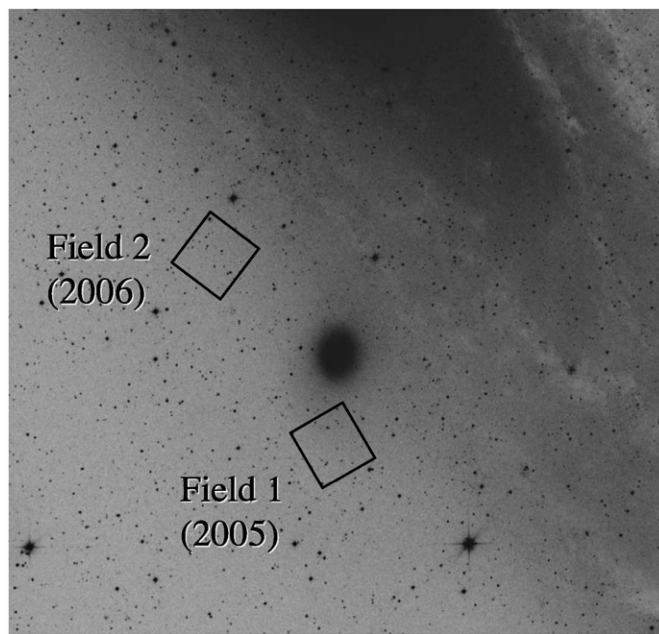


Figure 1. Location of our ACS fields overplotted on a digitized sky survey image in the region of M31. The dwarf elliptical galaxy M32 is near the center of the image. North is up and east is to the left.

are the parallel observations associated with each pointing obtained with the ACS Wide Field Channel (WFC) using the F606W ($\sim V$) filter. Table 1 provide some details of the observational data. The temporal coverage is 2.2 days for Field 1 and 3.1 days for Field 2.

Figure 1 shows the locations of these fields relative to M31. While the M32-background field was carefully selected to fall along the M31 isophote that ran through the M32 envelope field, the two fields were significantly separated in time, thus different spacecraft rolls between the two epochs caused the parallel WFC aperture to fall randomly about the primary HRC fields. Field 1 thus samples a region that is 4.5 kpc (in a projected distance) from the center of M31, while Field 2 is located 6.6 kpc from the center. Note that throughout this paper, we adopt an M31 distance modulus of $(m - M)_0 = 24.43$ corresponding to a distance of 770 kpc (Freedman & Madore 1990).

The spacecraft was dithered in a complex pattern to both achieve Nyquist sampling in the HRC and rejection of CCD defects. Each pair of orbits was dithered in a 2×2 square pattern of 0.5 HRC pixel steps, followed by larger steps to trace a skewed-square spiral of ~ 0.2 arcsec total amplitude over the 16 total orbits devoted to each filter/field combination. The subpixel dithering to achieve Nyquist sampling in the HRC is not optimal for the 2 times larger pixels of the WFC, but the larger scale dither pattern fortunately served to offer diverse sampling information for the parallel imagery.

3. REDUCTIONS

3.1. Photometry of Program Frames

We chose to work on the FLT images as retrieved from the *HST* archive. These frames have been bias subtracted and flat fielded, but, unlike the drizzled (DRZ) images, they retain the geometric distortions of ACS (Mahmud & Anderson 2008). Photometry was performed using the same procedure as Sarajedini et al. (2006). The first step is the application of geometric correction images to the Wide Field Channel 1 and 2 (WFC1 and WFC2, respectively) portions of the FLT images. After this step, the data quality maps are applied where the values of the bad pixels in the science images are set to a number well below the sky background to be sure the photometry software ignores those pixels. At this point, the resultant images are ready to be photometered.

The detection of the stellar profiles and the measurement of magnitudes were done with the DAOPHOT/ALLSTAR/ALLFRAME crowded-field photometry software (Stetson 1987, 1994). After the application of the standard FIND and PHOT routines to detect stars and perform aperture photometry on them, ALLSTAR was applied to each of the 32 images in order to derive well-determined positions for all of the stars. In this step and in subsequent ones involving the application of a point-spread function (PSF) in order to determine positions and magnitudes, we made use of the high signal-to-noise PSFs constructed by Sarajedini et al. (2006). The reader is referred to that paper for the details of the PSF construction process.

The stellar positions from the ALLSTAR runs were used to construct a coordinate transformation between each of the 32 images and these were used to combine all of the images into one master frame per field. This combined frame was then input into ALLSTAR, from which a master coordinate list of stellar profiles was constructed. The resultant coordinate list along with the spatial transformation between the images and the PSFs were used in ALLFRAME to derive magnitudes for all detected profiles on each image. At this point, the measurements on each of the individual frames were matched and only stars appearing on all 32 images were kept.

The standardization of the individual magnitudes proceeded in the following manner. First, the correction for the charge transfer efficiency problem was applied using the prescription of Reiss & Mack (2004). The magnitudes were then adjusted to a radius of 0.5 arcsec and corrected for exposure time. Offsets to an infinite radius aperture published by Sirianni et al. (2005) were then applied. Finally, the resultant values were calibrated to the VegaMAG system using the zero point for the F606W filter from Sirianni et al. (2005). A correction to this zero point amounting to 0.022 mag was applied as a result of a revised calibration of the ACS/WFC photometric performance by Mack et al. (2007). Each of our magnitude measurements is affected by three sources of systematic error: the uncertainty in the aperture corrections (± 0.02 mag), the error in the correction to infinite aperture (± 0.00 mag) for the F606W filter, and the error in the VegaMAG zero point (± 0.02 mag).

3.2. Characterization of the Variable Stars

For a given star with 32 magnitude measurements, we calculated the mean photometric error as returned by ALLFRAME ($\langle \sigma_{\text{err}} \rangle$) and the standard deviation of the measurements (σ_{sd}). For the first round of variable searching, we considered any star a candidate if $\sigma_{\text{sd}} / \langle \sigma_{\text{err}} \rangle \geq 3.0$. Approximately 3000 stars fit this criterion in each of our two fields.

These stars were then input into our template-fitting period-finding algorithm, which is based on the method used by Sarajedini et al. (2006) as originally formulated by Layden & Sarajedini (2000). We have taken the FORTRAN code written for the Layden & Sarajedini (2000) study and rewritten it using the Interactive Data Language (IDL) incorporating a graphical user interface (GUI). The original FORTRAN code used the “amoeba” minimum-finding algorithm exclusively, but our code, dubbed FITLC,⁶ has the option to use a more robust algorithm known as “pikaia” which has its roots in the study of genetics. The software uses 10 template light curves—six ab-type RR Lyraes, two c-type RR Lyraes, one eclipsing binary, and one contact binary. It searches over a period range from 0.2 day to a specified maximum (2.2 days for our Field 1 and 3.1 days for Field 2) looking for the period that minimizes the value of χ^2 . This is accomplished with a two-step process. First pikaia is used to find the combination of epoch, amplitude, and mean magnitude that minimize χ^2 at evenly spaced period increments of 0.01 day. Then pikaia is applied again to find the combination of epoch, amplitude, mean magnitude, and period that minimize χ^2 within ± 0.01 day of the period with the lowest χ^2 . The best fitting period from this final step is taken to be the period of the variable. The resultant phased light curves for each star were visually examined, and the stars that presented a compelling case for variability were retained in our final database. Of the ~ 6000 total stars originally fit, 752 exhibit genuine variability as shown by our data.

As a test of our template-fitting method, we have also applied the Lomb-Scargle period-finding algorithm (Scargle 1982; Horne & Baliunas 1986) to the time series photometry of the RR Lyraes in our sample. We find a mean difference of 0.0007 d in the periods determined by the two methods throughout the period range of RR Lyraes. In the minority of cases where template-fitting and Lomb-Scargle yield significantly different results, the resultant phased light curves are of significantly higher quality for the former method as compared with the latter. Furthermore, to test for the presence of aliasing effects in our derived periods, we have also examined fitted light curves using periods that correspond to χ^2 minima near half of the optimum period. In all cases, these fits are clearly inferior to the ones yielded by the optimum period from FITLC.

Tables 2 and 3 list the individual F606W magnitudes of each variable at each epoch wherein 2,450,000 has been subtracted from the epoch value, while Tables 4 and 5 list the candidate variables in our two fields along with their properties such as period, amplitude, and mean intensity-weighted magnitude. These stars fall into two broad categories. First, there are those that clearly show variability, but their periods are comparable to or longer than our observing window. These are referred to as “long period” in Tables 4 and 5. There is also one candidate anomalous Cepheid in our data set, which is so indicated in Table 5. The second category includes stars that exhibit clear periodic variability with a period that is significantly shorter than our observing window but longer than 0.2 d. These are the stars for which we can be confident of our periods. Some examples of stars with periods longer than our observing window are shown in Figure 2, while Figure 3 shows phased light curves of a number of contact and eclipsing binaries in our data set. Figure 4 displays the phased light curves of all of the RR Lyrae variables for which we have derived periods.

⁶ <http://www.astro.ufl.edu/~cmancone/fitlc.html>

Table 2
Raw Light Curves Field 1

Epoch	001 Mag	001 Err	002 Mag	002 Err	003 Mag	003 Err	004 Mag	004 Err	005 Mag	005 Err
3635.97534180	21.414	0.022	21.960	0.021	24.033	0.033	24.782	0.059	24.639	0.049
3635.99096680	21.417	0.024	21.984	0.017	24.023	0.033	24.826	0.052	24.664	0.049
3636.04003906	21.442	0.019	22.088	0.018	24.024	0.052	24.967	0.065	24.699	0.044
3636.05566406	21.400	0.028	22.032	0.025	24.011	0.021	24.650	0.052
3636.10693359	21.405	0.018	22.051	0.030	24.016	0.051	24.750	0.034	24.604	0.045
3636.12304688	21.384	0.030	22.083	0.027	24.013	0.042	24.582	0.038	24.585	0.046
3636.17358398	21.390	0.018	22.171	0.027	23.998	0.043	24.556	0.039
3636.18969727	21.384	0.025	22.118	0.028	24.607	0.056
3636.70800781	21.329	0.011	22.305	0.027	24.050	0.059	24.706	0.039	24.890	0.037
3636.72363281	21.321	0.016	22.332	0.036	24.036	0.036	24.755	0.031	24.799	0.042
3636.77294922	21.323	0.010	22.382	0.019	24.853	0.044	24.617	0.022
3636.78833008	21.315	0.015	22.339	0.029	24.037	0.035	24.846	0.048	24.552	0.049
3636.83959961	21.313	0.017	22.344	0.035	24.057	0.045	24.784	0.029	24.594	0.055
3636.85571289	21.312	0.024	22.356	0.019	24.018	0.056	24.754	0.058	24.618	0.049
3636.90625000	21.314	0.020	22.344	0.018	24.074	0.043	24.673	0.053	24.619	0.037
3636.92236328	21.288	0.021	22.366	0.040	24.061	0.036	24.554	0.033	24.523	0.054
3637.77368164	21.222	0.014	21.832	0.022	23.992	0.040	24.629	0.037	24.619	0.025
3637.78930664	21.198	0.016	21.805	0.021	24.012	0.022	24.553	0.036	24.640	0.026
3637.83862305	21.197	0.018	21.538	0.033	23.949	0.030	24.672	0.039	24.643	0.040
3637.85424805	21.209	0.011	21.542	0.023	23.994	0.037	24.704	0.048	24.649	0.045
3637.90551758	21.225	0.020	21.477	0.027	23.980	0.034	24.932	0.071	24.646	0.098
3637.92163086	21.192	0.021	21.498	0.028	23.977	0.030	24.875	0.050	24.617	0.062
3637.97216797	21.208	0.022	21.591	0.026	24.882	0.026	24.606	0.087
3637.98803711	21.208	0.014	21.541	0.023	23.987	0.031	24.841	0.044
3638.04028320	21.183	0.017	21.634	0.018	24.000	0.025	24.764	0.032	24.669	0.042
3638.05566406	21.180	0.020	21.655	0.025	24.007	0.025	24.673	0.050	24.594	0.071
3638.10498047	21.186	0.020	21.606	0.021	24.000	0.036	24.594	0.038	24.914	0.036
3638.12060547	21.165	0.015	21.644	0.033	24.063	0.022	24.587	0.026	25.073	0.057
3638.17187500	21.198	0.020	21.692	0.024	24.060	0.034	24.648	0.041	25.115	0.047
3638.18798828	21.173	0.014	21.730	0.031	24.031	0.043	24.639	0.028	25.236	0.091
3638.23852539	21.184	0.015	21.732	0.022	24.043	0.073	24.754	0.025	24.946	0.068
3638.25463867	21.158	0.019	21.750	0.026	24.086	0.035	24.760	0.038	24.909	0.035

All of the stars that exhibit RR Lyrae light curves also have apparent magnitudes in the range one would expect if they are at the distance of M31. Therefore, it is reasonable to assume that most if not all of these objects are RR Lyrae stars belonging to M31 and/or its environs. This assertion will become clearer when we compare the luminosity function (LF) of the nonvariable stars with that of the RR Lyraes.

It should be noted that we are much less confident about the properties of the eclipsing and contact binaries that we have identified as compared with the RR Lyraes. This is because we know what period range to expect for the RR Lyraes (~ 0.25 d to ~ 0.90 d), so that our observing window provides coverage of multiple cycles of variation for a given RR Lyrae star. In contrast, the periods of the eclipsing and contact binaries cannot be similarly constrained, so it is difficult for us to ensure that our observing window is sufficient to derive the periods of these variables. As such, we have provided information for these stars (positions, periods, amplitudes, and magnitudes) so that future observers can confirm the nature of their variability, but we will not consider them further here. Instead, for the remainder of this paper, we will limit our discussion to the 681 RR Lyrae variables in our sample and what they reveal about the properties of the M31 system.

3.3. Light Curve Simulations

In order to characterize the possible biases in the derived periods of our variable star sample, we have performed simulations

of our light-curve-fitting technique in the following manner. For the ab-type RR Lyraes, we selected one of the light curve templates (the results are insensitive to the actual ab-type template used) and produced artificial variables with a period range of 0.45–0.80 days and amplitudes between 0.3 and 1.3 mag. For the c-type RR Lyraes, a period range of 0.25–0.40 days and an amplitude range of 0.2–0.5 mag were used. One thousand variables were generated in each case, and the mean photometric error at the level of the RR Lyraes was used to populate the light curves using the same observing window as the actual data. These simulated light curves were input into our template light-curve-fitting software. We are interested in comparing the input periods with the output periods in order to gauge any possible biases present in our analysis method.

Figures 5 (RRab) and 6 (RRc) show the result of these fits for Field 1 wherein the upper panel shows the mean difference between the input and output periods, while the lower panel illustrates the differences in the period distributions. The results of the simulations for RR Lyraes in Field 2 are indistinguishable from those in Field 1. Of the 1000 ab-type RR Lyraes generated, none were mistaken for any other type of variable among the 10 light curve templates used in the fitting. For the c-type light curves, two of the 1000 generated variables were fit with a contact binary template. We find no significant biases in our determination of the periods for both types of RR Lyraes. As such, we will not apply any sort of correction to our derived periods. As for the errors in the period and amplitude determinations, these simulations suggest that an individual ab-type RR Lyrae has an error of ± 0.005 day and ± 0.044 mag,

Table 3
Raw Light Curves Field 2

Epoch	366 Mag	366 Err	367 Mag	367 Err	368 Mag	368 Err	369 Mag	369 Err	370 Mag	370 Err
3775.87866211	21.896	0.034	22.464	0.029	22.360	0.038	23.676	0.023
3775.89428711	21.955	0.031	22.409	0.050	22.387	0.038	23.583	0.025	23.667	0.036
3775.94409180	21.901	0.024	22.388	0.041	22.347	0.028	23.624	0.024	23.597	0.026
3775.95971680	21.885	0.035	22.443	0.029	22.342	0.038	23.626	0.026	23.664	0.030
3776.01098633	21.930	0.028	22.417	0.043	22.347	0.029	23.686	0.027	23.607	0.020
3776.02685547	21.881	0.034	22.400	0.032	22.387	0.032	23.689	0.036	23.579	0.036
3776.07763672	21.886	0.027	22.384	0.032	22.391	0.035	23.716	0.026	23.584	0.033
3776.09350586	21.914	0.019	22.323	0.063	22.332	0.028	23.688	0.037	23.592	0.022
3777.54418945	21.748	0.044	22.178	0.041	22.234	0.034	23.806	0.070	23.671	0.035
3777.55957031	21.693	0.035	22.174	0.054	22.178	0.030	23.807	0.063	23.741	0.034
3777.60913086	21.706	0.034	22.179	0.049	22.159	0.029	23.836	0.053	23.740	0.041
3777.62475586	21.722	0.043	22.174	0.040	22.053	0.060	23.872	0.066	23.707	0.034
3777.67602539	21.692	0.053	22.166	0.045	22.150	0.029	23.863	0.029	23.698	0.029
3777.69189453	21.711	0.063	22.149	0.033	22.140	0.036	23.888	0.040	23.719	0.042
3777.74243164	21.710	0.060	22.160	0.025	22.158	0.028	23.858	0.029	23.672	0.047
3777.75854492	21.679	0.049	22.156	0.041	22.152	0.029	23.855	0.033	23.664	0.023
3778.41113281	21.662	0.028	22.085	0.020	22.113	0.024	23.397	0.020	23.635	0.055
3778.47485352	21.656	0.032	22.074	0.020	22.128	0.033	23.454	0.029	23.702	0.061
3778.54150391	21.652	0.033	22.067	0.026	22.113	0.035	23.553	0.036	23.899	0.056
3778.55712891	21.636	0.032	22.065	0.024	22.097	0.023	23.515	0.026	23.905	0.059
3778.60839844	21.589	0.043	22.055	0.034	22.081	0.035	23.567	0.030	23.981	0.032
3778.62451172	21.614	0.025	22.052	0.039	22.085	0.033	23.594	0.029	23.941	0.027
3778.67504883	21.618	0.032	22.055	0.035	22.087	0.030	23.584	0.023	23.783	0.038
3778.69116211	21.599	0.044	22.045	0.035	22.059	0.042	23.632	0.034	23.834	0.034
3778.74340820	21.592	0.028	22.056	0.038	22.077	0.036	23.671	0.023	23.735	0.026
3778.75903320	21.609	0.034	22.041	0.031	22.054	0.059	23.721	0.025	23.815	0.040
3778.80786133	21.600	0.027	22.030	0.022	22.055	0.036	23.723	0.018	23.653	0.020
3778.82348633	21.594	0.028	22.053	0.036	22.016	0.036	23.746	0.020	23.687	0.031
3778.87475586	21.581	0.029	22.049	0.045	22.038	0.031	23.779	0.029	23.656	0.021
3778.89086914	21.608	0.025	22.047	0.039	22.029	0.032	23.814	0.030	23.659	0.020
3778.94140625	21.597	0.013	22.040	0.041	22.044	0.023	23.835	0.024	23.638	0.019
3778.95751953	21.597	0.025	22.032	0.038	22.045	0.034	23.845	0.029	23.667	0.028

Table 4
Field 1 Variable Stars

Star ID	R.A. (J2000)	Decl. (J2000)	Period (Days)	m_{F606W} Amplitude	$\langle m_{F606W} \rangle$	Type
1	0 42 38.35	40 47 8.3	1.551	0.301	21.337	long period
2	0 42 41.92	40 45 19.1	2.559	0.919	22.070	long period
3	0 42 37.94	40 45 18.9	1.408	0.100	24.029	long period
4	0 42 34.90	40 46 4.3	0.387	0.288	24.712	RRc
5	0 42 42.82	40 45 23.6	1.561	0.490	24.685	Eclipsing
6	0 42 34.49	40 46 29.0	1.400	0.246	24.758	Contact
7	0 42 41.61	40 46 7.4	0.660	0.725	24.877	RRab
8	0 42 42.42	40 44 59.8	1.539	0.160	24.820	long period
9	0 42 43.09	40 44 59.0	0.508	0.575	24.859	RRab
10	0 42 36.11	40 47 13.9	2.188	0.130	24.918	long period

(This table is available in its entirety in machine-readable and Virtual Observatory (VO) forms in the online journal. A portion is shown here for guidance regarding its form and content.)

respectively. For a c-type RR Lyrae star, these error values are ± 0.001 day and ± 0.022 mag.

4. RESULTS

4.1. Luminosity Functions

Figure 7 displays a comparison of the LFs of the nonvariable stars in the two fields. Both distributions feature a quick rise from brighter magnitudes to fainter ones with a pronounced peak at $m_{F606W} \sim 25.3$ representing the core-helium burning horizontal branch (HB) stars. A sudden drop in both LFs at $m_{F606W} \sim 27.7$ suggests the onset of significant incompleteness as the limit of the photometry is approached. The fact that the HB stars

are more than 2 magnitudes brighter than this completeness threshold indicates that our sample of RR Lyrae variable candidates should not be adversely biased by photometric incompleteness.

The two panels of Figure 8 compare the LF of the nonvariable stars with those of the RR Lyraes in the two observed fields. We have used the intensity-weighted magnitudes listed in Tables 4 and 5 to construct these distributions. Gaussian fits to the regions around the RR Lyrae LF peaks yield $\langle m_{F606W} \rangle = 25.20 \pm 0.04$ for Field 1 and $\langle m_{F606W} \rangle = 25.22 \pm 0.04$ for Field 2, where the errors represent the standard error of the mean combined with the uncertainty in the photometric zero point added in quadrature. For the nonvariable stars, these peaks correspond

Table 5
Field 2 Variable Stars

Star ID	R.A. (J2000)	Decl. (J2000)	Period (Days)	m_{F606W} Amplitude	$\langle m_{F606W} \rangle$	Type
366	0 43 17.55	40 58 42.3	1.886	0.314	21.732	long period
367	0 43 20.31	40 58 12.1	2.234	0.387	22.141	long period
368	0 43 24.43	40 56 27.8	2.220	0.288	22.146	long period
369	0 43 24.57	40 56 51.9	1.366	0.501	23.625	long period
370	0 43 16.06	40 58 29.2	1.978	0.291	23.675	Eclipsing
371	0 43 23.53	40 57 3.9	0.557	0.558	23.794	RRab
372	0 43 30.90	40 56 53.4	2.575	0.794	24.014	long period
373	0 43 17.54	40 58 48.8	1.142	0.839	24.299	Eclipsing
374	0 43 20.14	40 57 30.7	2.570	0.368	24.386	Contact
375	0 43 20.79	40 57 27.2	0.600	0.563	24.454	RRab

(This table is available in its entirety in machine-readable and Virtual Observatory (VO) forms in the online journal. A portion is shown here for guidance regarding its form and content.)

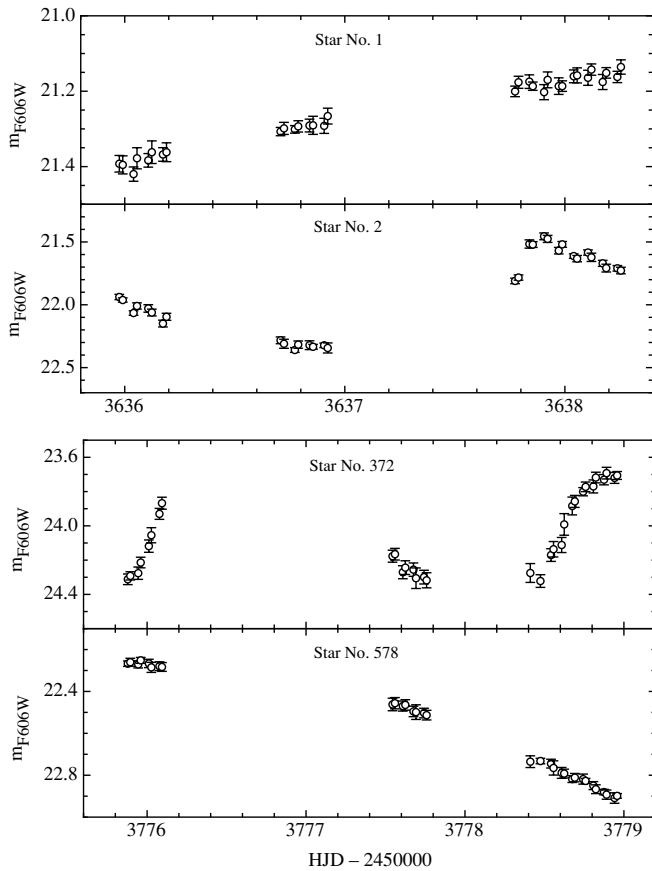


Figure 2. Unphased light curves for a sample of our variable stars with periods that are comparable to or longer than our observing window. The numbers refer to the stars in Tables 4 and 5.

to $\langle m_{F606W} \rangle = 25.25 \pm 0.04$ for Field 1 and $\langle m_{F606W} \rangle = 25.23 \pm 0.04$ for Field 2. The $1\text{-}\sigma$ width of these distributions is ~ 0.11 mag. These numbers suggest no significant difference in the mean magnitudes of the RR Lyraes and the nonvariable stars. This serves to confirm our assertion that most if not all of the variable stars in this magnitude range are RR Lyrae variables. In addition, when we combine the RR Lyrae variables from both fields, we find a mean magnitude of $m_{F606W} = 25.21 \pm 0.01$ on the VEGAmag system. The quoted uncertainty represents the standard error of the mean. When converted to the V band using the mean offset for RR Lyraes in the middle of the instability strip from B2004 of $V - m_{F606W} = 0.08 \pm 0.04$, we derive

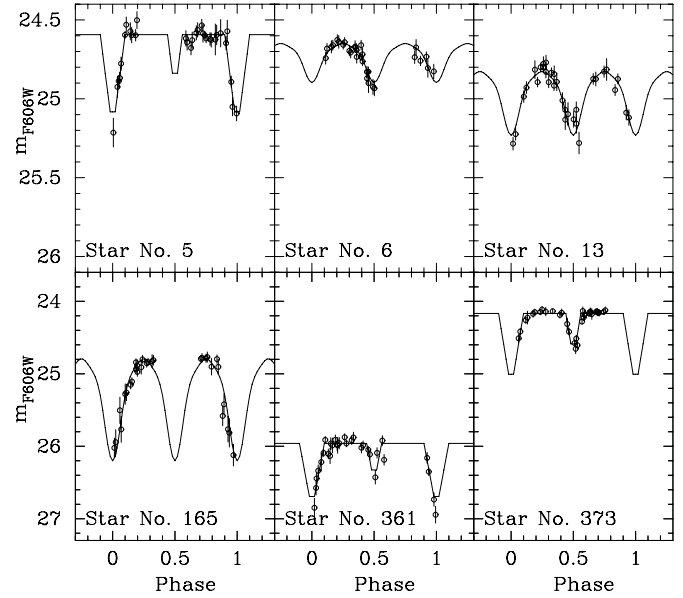


Figure 3. Phased light curves for some of the contact and eclipsing binaries identified in this study.

$\langle V(RR) \rangle = 25.29 \pm 0.01$ (random) ± 0.05 (systematic). This compares favorably with the value of $\langle V(RR) \rangle = 25.30 \pm 0.01$ based on the average for the ab-type and c-type RR Lyraes from the B2004 study (see Figure 8). We note in passing that a Gaussian fit to the LF of the B2004 RR Lyraes yields a 1σ width of 0.12 mag, which is comparable to the value for the RR Lyraes in the present study.

4.2. Number Ratios

Of the 681 total RR Lyrae stars in our sample, 555 (267 in Field 1 and 288 in Field 2) are of the ab-type with the remainder being c-type (57 in Field 1 and 69 in Field 2). This leads to a ratio of $N_c/N_{abc} = 0.19 \pm 0.02$, which is quite different than the value of $N_c/N_{abc} = 0.46 \pm 0.11$ inferred from the B2004 data. Therefore, our samples of ab-type and c-type RR Lyraes are a factor of ~ 2 greater and a factor of ~ 2 less, respectively, than what we would expect based on the B2004 field. Taken at face value, this suggests that the old population in the environs of M31 exhibits different pulsation properties at 4–6 kpc as compared with 11 kpc.

To evaluate the validity of this assertion, we need to address the question of incompleteness in our sample of RR

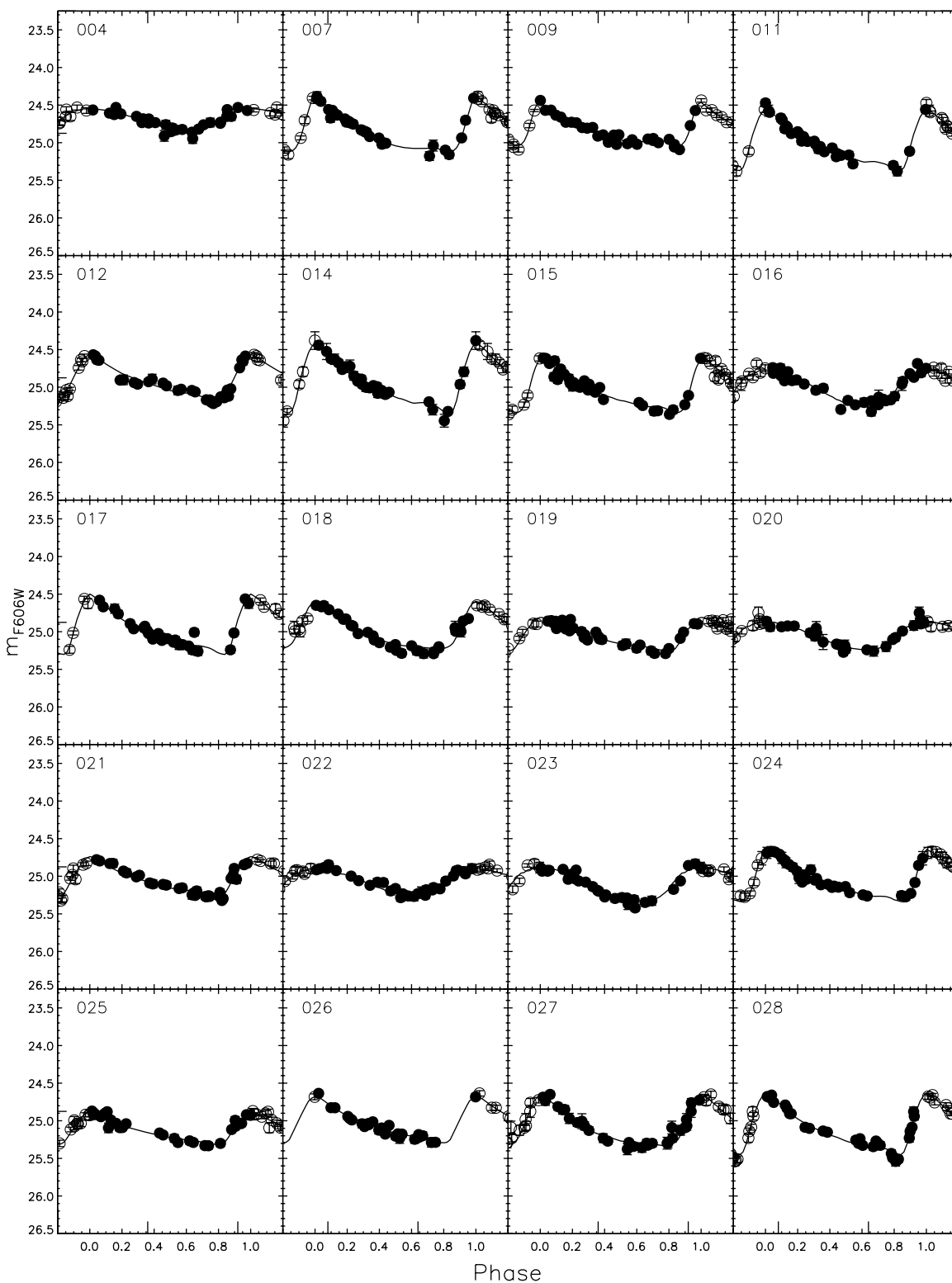


Figure 4. Phased light curves for the 681 RR Lyrae variables identified in this study. The open circles are repeated to complete the light curve for phase less than zero and greater than 1.

(The complete figure set (35 images) is available in the online journal.)

Lyraes. Are there significant numbers of RR Lyraes in our fields that we have failed to identify? We begin by noting that B2004 claim that their samples of c-type and ab-type RR Lyraes are complete and not significantly contaminated by dwarf Cepheids. Therefore, we can gain some insight by

comparing the amplitude distributions of the B2004 RR Lyrae variables with our sample as shown in Figure 9. This comparison suggests that the amplitude distribution of the B2004 RR Lyraes is consistent with those of our sample. Application of the Kolmogorov–Smirnov test to these distributions confirms this

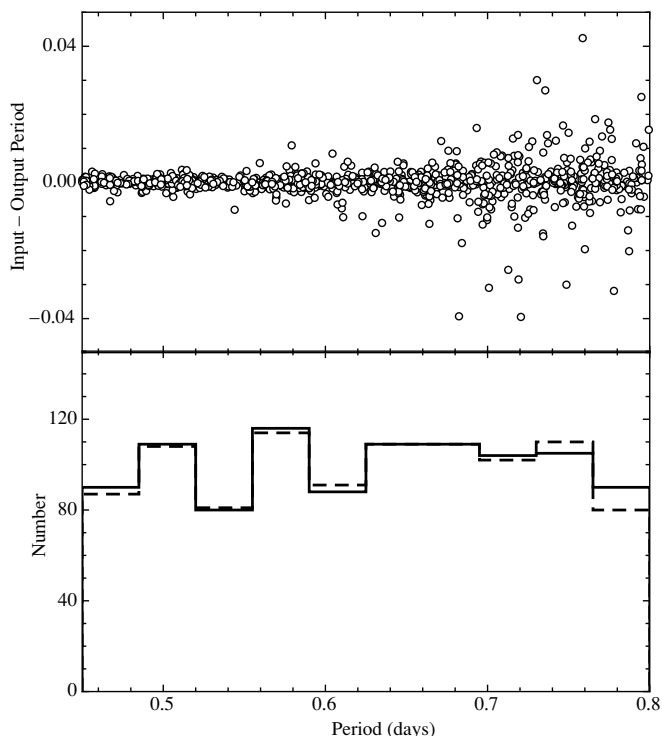


Figure 5. Results of the light curve simulations performed in order to characterize any biases in our period-finding algorithm in the case of the RRab variables. The upper panel plots the variation of input minus recovered period, while the lower panel plots the period distribution both as a function of period in days. The solid line is the input distribution, while the dashed line represents the recovered one. These simulations suggest that the combination of the input data and the period-finding algorithm does not introduce significant biases in our derived periods.

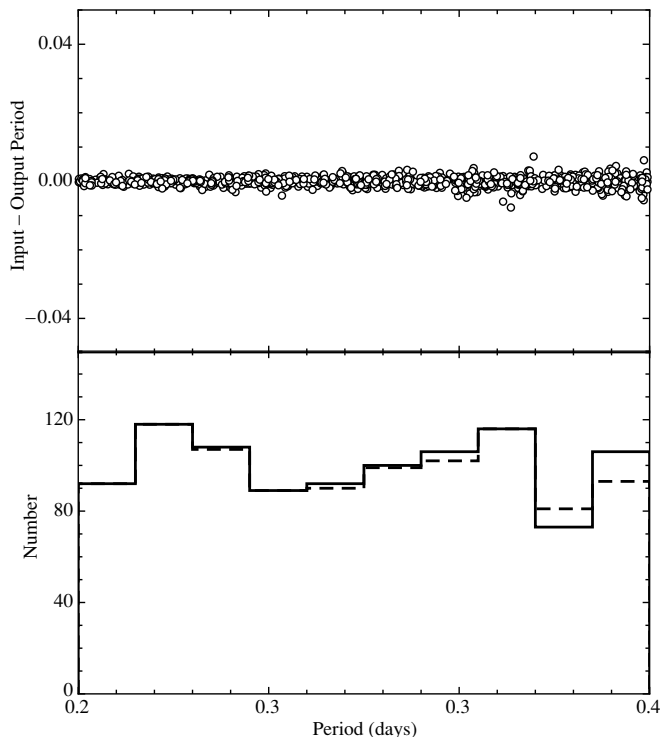


Figure 6. Same as Figure 5 except that the simulations have been performed using an c-type RR Lyrae variable light curve.

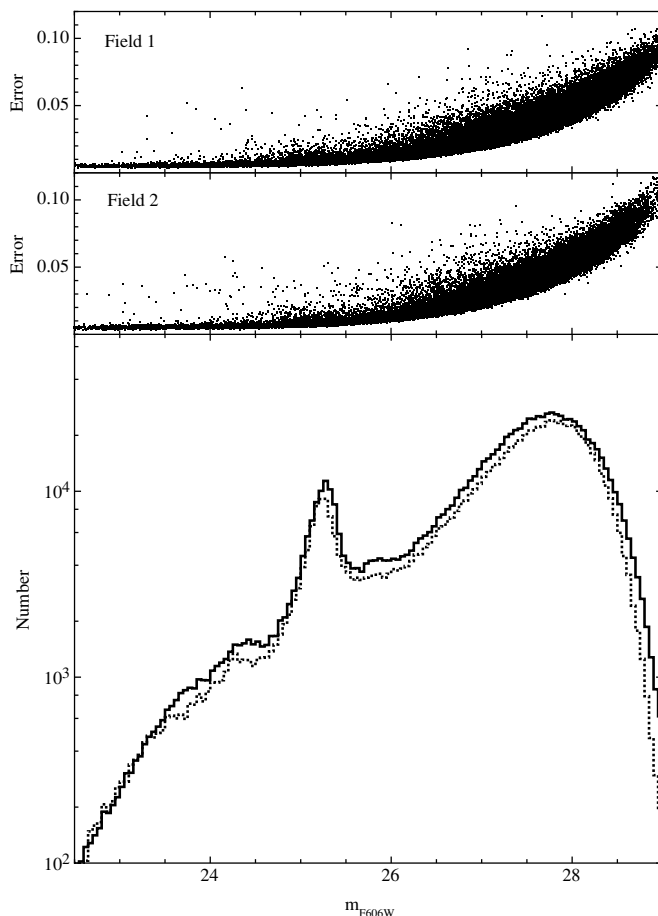


Figure 7. Luminosity functions for the nonvariable stars in the two fields studied herein. The solid line in the lower panel is the F606W band LF for the field observed in 2005 (field 1 in Table 1), while the dashed line is the LF for the region observed in 2006 (field 2 in Table 1). The two upper panels show the variation of the photometric error as output by ALLFRAME with magnitude. We have plotted every 10th point to make the appearance of these plots manageable.

suggestion. The fact that, at the low-amplitude end, the two distributions are not substantially different argues that significant numbers of low-amplitude RR Lyraes are not missing from our sample.

Another possibility of explaining the differences in the N_c/N_{abc} ratio between our fields and the one at 11 kpc is that our Field 1 data are significantly influenced by the stellar populations of M32 and not M31. In fact, we find $N_c/N_{abc} = 0.18 \pm 0.025$ in Field 1 and $N_c/N_{abc} = 0.19 \pm 0.025$ in Field 2, which are statistically indistinguishable from each other. In addition, the density of RR Lyrae variables and their period distributions are indistinguishable between Fields 1 and 2. For example, for the ab-type variables, Field 1 exhibits a mean period of $\langle P_{ab} \rangle = 0.553 \pm 0.004$, while Field 2 shows $\langle P_{ab} \rangle = 0.561 \pm 0.005$. In the case of the c-type RR Lyraes, the analogous values are $\langle P_c \rangle = 0.326 \pm 0.005$ and $\langle P_c \rangle = 0.327 \pm 0.004$, respectively. These values suggest that both of our fields sample the regions around M31 and are minimally contaminated by M32 RR Lyraes.

If this difference in the N_c/N_{abc} ratio between a radial distance of 11 kpc and 4–6 kpc in M31 is real, then it suggests that the RR Lyraes at 11 kpc are more akin to their brethren in Oosterhoff type II globular clusters, while those at 4–6 kpc are more like RR Lyraes in Oosterhoff type I clusters. This is based on the findings of Castellani et al. (2003) who examined the

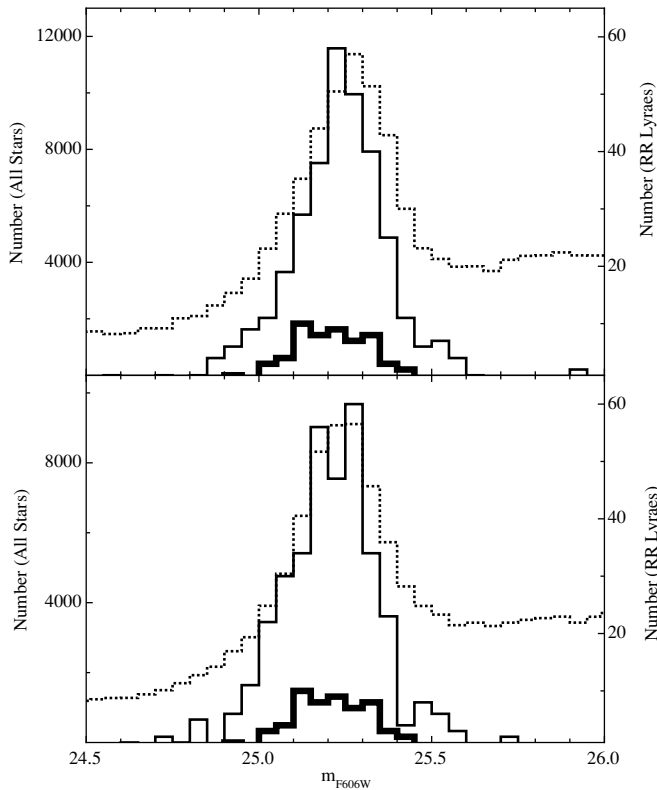


Figure 8. Luminosity functions for the nonvariable stars (dashed lines) compared with those of the RR Lyrae candidates (thin solid lines) in the two fields studied herein (see Table 1). The thicker solid lines represent the RR Lyrae stars from the study of Brown et al. (2004).

N_c/N_{abc} ratio in Galactic globulars. They found that among the 12 clusters with 40 or more variables, $\langle N_c/N_{abc} \rangle = 0.37$ for Oosterhoff II clusters and $\langle N_c/N_{abc} \rangle = 0.17$ for those of Oosterhoff type I. These compare favorably with the values of $\langle N_c/N_{abc} \rangle = 0.46$ for the 11 kpc field and $\langle N_c/N_{abc} \rangle = 0.19$ for the 4–6 kpc field.

4.3. Periods, Amplitudes, and Metallicities

The Bailey diagram for our sample of RR Lyraes is shown in Figure 10 where we plot the variables in the two fields using different colors. However, it is clear that they occupy the same regions of this diagram. The ab-type RR Lyrae variables are shown with open circles, while the c-type stars are plotted as open triangles. The dashed line in Figure 10 represents the relation exhibited by the RRAb stars in the B2004 field. The solid lines are the relations for Oosterhoff I and II globular clusters from Clement (2000). These lines have been adjusted to account for the difference between an amplitude in the V band and one in the $F606W$ band. Interestingly, the B2004 RR Lyrae relation is closer to the OoI line, even though the N_c/N_{abc} ratio in the B2004 field is closer to that of OoII clusters. It is unclear why this should be the case.

The B2004 line appears to be offset compared with our data suggesting slightly shorter periods for the RRAb variables in our fields. This behavior is further exemplified in Figure 11 which shows the period distributions in the two fields compared with the mean periods of the ab- and c-type RR Lyraes from B2004. We find mean periods of $\langle P_{ab} \rangle = 0.557 \pm 0.003$ and $\langle P_c \rangle = 0.327 \pm 0.003$. For the B2004 field, these values are $\langle P_{ab} \rangle = 0.594 \pm 0.015$ and $\langle P_c \rangle = 0.316 \pm 0.007$. The mean periods of the c-type variables are statistically indistinguishable

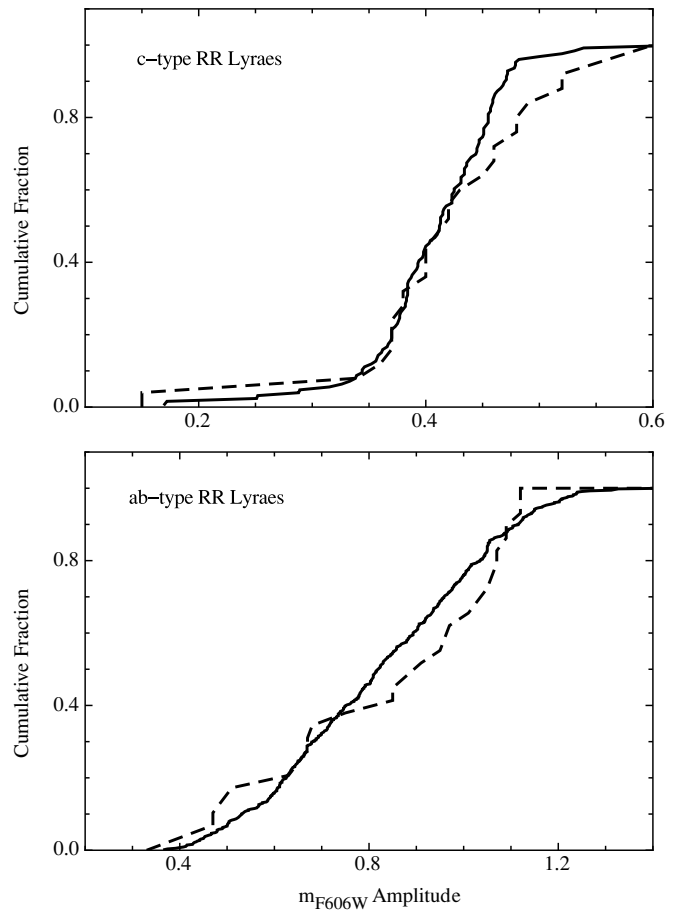


Figure 9. Upper panel shows the amplitude distribution of the c-type RR Lyraes from the present study (solid line) and the work of Brown et al. (2004, dotted line) scaled to the same maximum. The lower panel is the same as the upper one except that the ab-type RR Lyraes are plotted.

from each other, but the ab-types in our fields exhibit a somewhat shorter period as compared with those in the B2004 fields.

It is well known that as the metallicity of ab-type RR Lyraes increases, their periods decrease (e.g., Sandage 1993; Layden 1995; Sarajedini et al. 2006). Thus, the period distribution of these stars (Figure 11) can be converted to a metallicity distribution using equations derived by previous investigators. Using the data of A. C. Layden (2005, private communication) for 132 Galactic RR Lyraes in the solar neighborhood, Sarajedini et al. (2006) established a relation between period and metal abundance of the form

$$[\text{Fe}/\text{H}] = -3.43 - 7.82 \text{Log } P_{ab}. \quad (1)$$

This equation does not take into account the amplitudes of the RR Lyraes even though, as Figure 10 shows, there is a relation between amplitude and period for the ab-types. The work of Alcock et al. (2000) yielded a period–amplitude–metallicity relation of the form

$$[\text{Fe}/\text{H}] = -8.85[\text{Log } P_{ab} + 0.15A(V)] - 2.60, \quad (2)$$

where $A(V)$ represents the amplitude in the V band. We applied an 8% increase to the m_{F606W} amplitudes to convert them to V band values (B2004). Figure 12 shows the metallicity distribution function (MDF) for the ab-type RR Lyraes. The top panel compares the results obtained using Equations (1) and

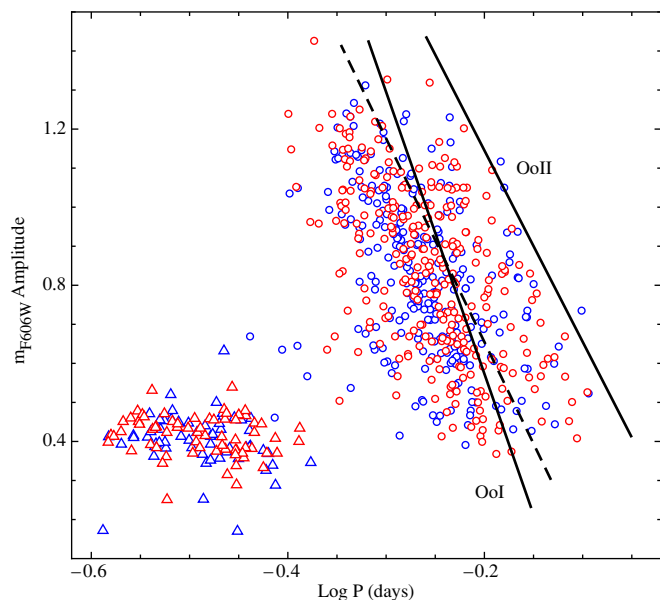


Figure 10. Bailey diagram for the RR Lyrae candidates in our fields. The open circles are the ab-type RR Lyraes, while the open triangles represent the c-type variables. The color coding represents the field number with blue being stars observed in field 1 and red those found in field 2. This plot shows that while the ab- and c-type RR Lyraes occupy their characteristic locations in this diagram, there is no significant difference between the RR Lyraes in the two observed fields. The dashed line shows the relation exhibited by the RRab stars in the field observed by Brown et al. (2004). The solid lines are the relations for Oosterhoff type I and II globular clusters from Clement (2000). These lines have been adjusted to account for the difference between an amplitude in the V band and one in the F606W band.

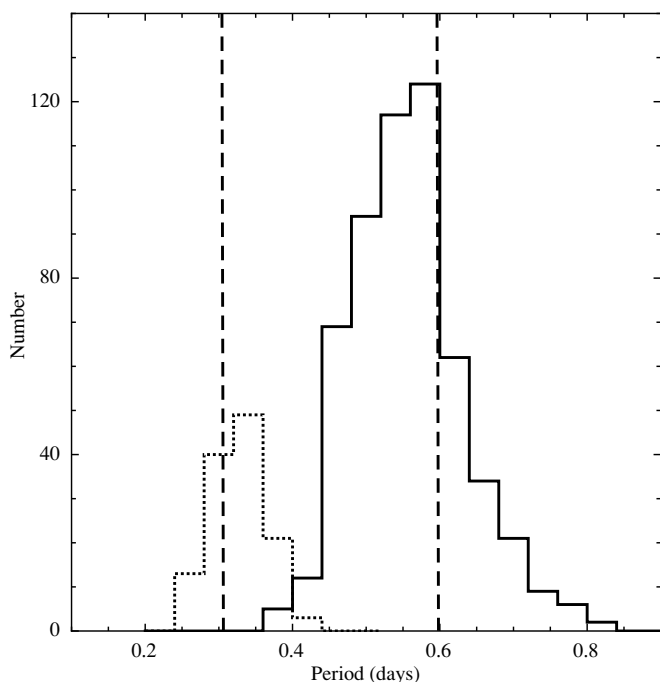


Figure 11. Period distributions of the ab-type (solid) and c-type (dotted) RR Lyrae variables. The dashed vertical lines represent the mean periods of these same stars from Brown et al. (2004). While the mean periods of the c-type variables agree between our study and that of Brown et al. (2004), the mean period of the ab-type RR Lyraes is somewhat shorter in our sample as compared with that of Brown et al.

(2), while the lower panel compares the MDFs for the two fields using Equation (2).

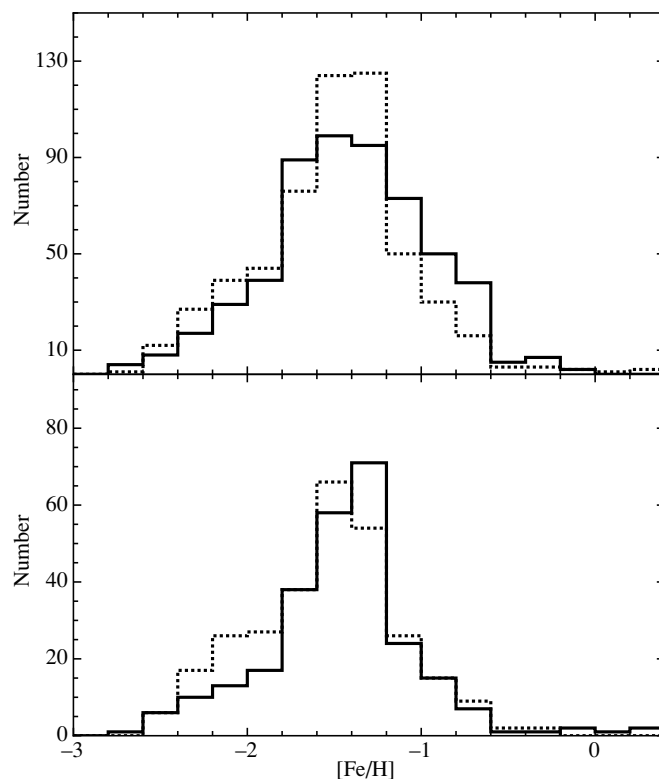


Figure 12. Upper panel shows the metallicity distribution function for our sample of RRab variables using two different formulations for the conversion between period and metal abundance (solid line—Equation (1), dashed line—Equation (2)). The lower panel shows the MDFs derived using Equation (2) for the two observed fields (dashed line—Field 2, solid line—Field 1).

We see in the upper panel of Figure 12 that, while the two MDFs exhibit very similar peak metallicities, the MDF generated using Equation (2) displays a more prominent peak. This is the representative of the fact that Equation (2) accounts for the variation of period with amplitude as well as metallicity resulting in a cleaner abundance signature in the MDF. In the lower panel of Figure 12, we see that the peaks of the RR Lyrae MDFs in our two fields differ by ~ 0.1 dex; we find $\langle [\text{Fe}/\text{H}] \rangle = -1.46 \pm 0.03$ for Field 1 and $\langle [\text{Fe}/\text{H}] \rangle = -1.54 \pm 0.03$ for Field 2, where the errors represent standard errors of the mean. This difference is not statistically significant.

Combining the RR Lyraes in the two fields yields the MDF shown as the solid line in Figure 13, wherein the binned and generalized histograms are shown. The latter has been constructed using an error of 0.31 dex per star (Alcock et al. 2000). The peak metallicity for our sample of ab-type RR Lyraes is then $\langle [\text{Fe}/\text{H}] \rangle = -1.50 \pm 0.02$, where the error is the standard error of the mean. The systematic error of this measurement is likely to be closer to ~ 0.3 dex. The dotted distributions in Figure 13 are the binned and generalized histograms for the RRab stars in the sample of B2004 scaled to the same number of ab-type RR Lyraes as in our fields. The peak abundance of this MDF is $\langle [\text{Fe}/\text{H}] \rangle = -1.77 \pm 0.06$.

There are three observations we can make regarding the appearance of Figure 13. First, it would seem that the errors on the individual metallicity measurements are significant enough to overwhelm any fine structure that may be present in the two MDFs. That is to say, both MDFs look essentially like normal distributions. Second, since we have applied the same transformation from period to metallicity to both sets of RR Lyraes, we can assert with significant statistical certainty that

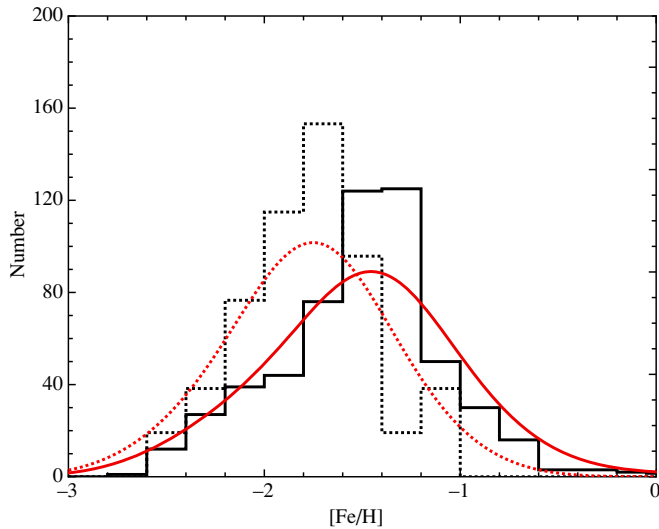


Figure 13. Comparison of the metallicity distribution function derived from the ab-type RR Lyraes from the present study (solid lines) and those from the Brown et al. (2004) study (dotted lines). The latter has been scaled to match the number of ab-type RR Lyraes in our two fields. Both binned and generalized histograms are shown.

the mean metal abundance of the RR Lyraes in the B2004 field is lower than that of the RR Lyraes in our two fields. This difference amounts to $\Delta[\text{Fe}/\text{H}] = 0.27 \pm 0.06$ and reflects back on the period shift seen in the Bailey diagram shown in Figure 10. Third, there are a small but non-negligible number of ab-type RR Lyraes with metallicities above $[\text{Fe}/\text{H}] \sim -1$ that are not seen in the B2004 field. Given the fact that our field is closer to the central regions of M31 as compared with the B2004, it is possible that these metal-rich RR Lyraes could belong to the bulge or disk of M31. We return to this point in the following section.

One last point needs to be addressed before leaving this section and that is concerned with the M31 distance implied by the RR Lyraes in our sample. Using the relation advocated by Chaboyer (1999) of $M_V(\text{RR}) = 0.23[\text{Fe}/\text{H}] + 0.93$ and a reddening of $E(B - V) = 0.08 \pm 0.03$ (Schlegel et al. 1998), we find a distance modulus of $(m - M)_0 = 24.46 \pm 0.11$. This is consistent with the B2004 value and a number of previous determinations.

5. DISCUSSION

We now seek to place our RR Lyrae abundance results within the broader context of the projected radial metallicity distribution of various populations in the environs of M31. Figure 14 shows this information for a range of stellar populations in and around M31. The metallicities for the RR Lyraes in the two fields considered herein are shown by the filled circles, while the open circle represents the RR Lyraes in the B2004 field. The inner-most point is the bulge metallicity from the work of Sarajedini & Jablonka (2005), while the remaining open squares are the bulge/halo points from the work of Kalirai et al. (2006) as shown in their Table 3. The dashed line is the least-squares fit to the open squares with a slope of -0.75 ± 0.11 . The other points represent the dwarf spheroidal companions to M31 (crosses, Grebel et al. 2003; Koch & Grebel 2006), the globular cluster G1 (filled square, Meylan et al. 2001), and the furthest globular cluster in M31 (open triangle, Martin et al. 2006). Note that we have adopted the mean metallicity of M32 from the work of Grillmair et al. (1996). The elongated rectangle represents the locations of the halo globular clusters in M33 from Sarajedini

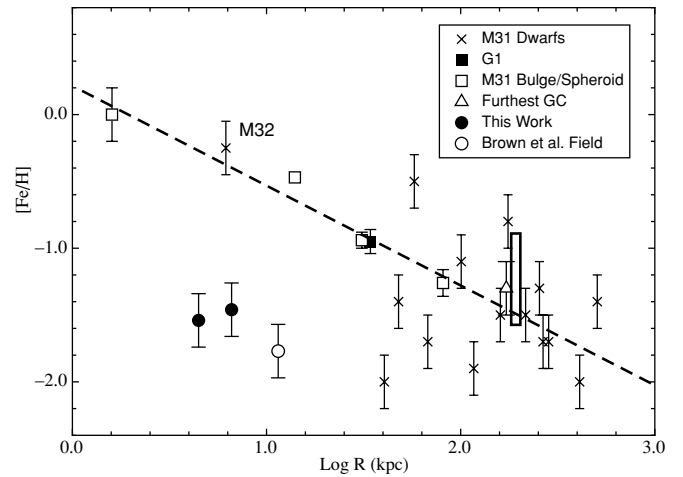


Figure 14. Plot of the variation of metal abundance with a projected distance from the center of M31. Our results are shown by the filled circles, while the mean metallicity of the RR Lyraes studied by Brown et al. (2004) is indicated by the open circle. The inner most open square represents the bulge abundance measured by Sarajedini & Jablonka (2005). The remaining open squares are the bulge/halo points from the work of Kalirai et al. (2006). The dashed line is the least-squares fit to these data with a slope of -0.75 ± 0.11 . The crosses represent the dwarf galaxies surrounding M31 from the work of Grebel et al. (2003) and Koch & Grebel (2006), whereas the abundance of M32 is taken from Grillmair et al. (1996). The filled square is the well known massive globular cluster G1 studied by Meylan et al. (2001). The open triangle is the furthest known globular cluster in M31 discovered by Martin et al. (2006). For completeness, the boxed region shows the location of the halo globular clusters in M33 from the work of Sarajedini et al. (2000). All of these points have been scaled to an M31 distance of $(m - M)_0 = 24.43$.

et al. (2000). All of these values are based on a distance of $(m - M)_0 = 24.43$ (770 kpc) for M31. In cases where an error in the metallicity is not available, we have adopted a value of ± 0.2 dex.

We see in Figure 14 a clear representation of the notion that the halo population in M31 does not begin to dominate until a galactocentric distance of ~ 30 kpc, as suggested by a number of authors (Guhathakurta et al. 2005; Irwin et al. 2005; Kalirai et al. 2006; Koch et al. 2008). At this location, we see a transition region between the globular cluster G1 which is consistent with the inner-spheroid metallicity gradient (dashed line) and the dwarf spheroidal galaxies which show no relation between abundance and galactocentric distance. In this sense, it would appear that the RR Lyrae populations in our field and that of B2004 follow the trend outlined by the stellar populations outside of ~ 30 kpc. This suggests that the RR Lyraes at these locations are probably members of the M31 halo rather than its bulge suggesting that the halo can be studied as close as 4 kpc from the center of M31 by focusing on the RR Lyraes.

6. SUMMARY AND CONCLUSIONS

We have presented F606W ($\sim V$) observations from the *HST* archive taken with the Advanced Camera for Surveys of two fields located 4–6 kpc from the center of M31. In these regions, we identify 752 variable stars of which 681 are likely to be *bona fide* RR Lyraes. From the properties of these stars, we draw the following conclusions.

1. The mean magnitude of the RR Lyrae stars is $\langle V \rangle = 25.29 \pm 0.05$ where the uncertainty combines both the random and systematic errors. This is in good agreement with the results of Brown et al. (2004).
2. The ratio of c-type RR Lyraes to all types is reminiscent of the RR Lyraes in Oosterhoff type I globular clusters in

the Milky Way. This ratio is significantly different than the Brown et al. (2004) field at 11 kpc from the center of M31 wherein this ratio is closer to that of Oosterhoff II clusters.

3. When the periods and amplitudes of the ab-type RR Lyraes in our sample are interpreted in terms of metallicity, we find the metallicity distribution function to be indistinguishable from a Gaussian with a peak at $\langle[\text{Fe}/\text{H}]\rangle = -1.50 \pm 0.02$, where the error is the standard error of the mean. The same analysis applied to the Brown et al. (2004) RR Lyraes yields a peak of $\langle[\text{Fe}/\text{H}]\rangle = -1.77 \pm 0.06$.
4. Using the RR Lyrae luminosity–metallicity relation advocated by Chaboyer (1999) and a reddening of $E(B - V) = 0.08 \pm 0.03$, we find a distance modulus of $(m - M)_0 = 24.46 \pm 0.11$ for M31.
5. We examine the radial metallicity gradient in the environs of M31 using published values for the bulge and halo of M31 as well as the abundances of the dwarf spheroidal companions and globular clusters of M31. In this context, despite the relative proximity of the RR Lyraes in the present study to the center of M31, their metal abundance is more reminiscent of a halo population than a bulge or disk. Therefore, by using the RR Lyraes as a proxy, the halo can be studied as close as 4 kpc from the center of M31.

We are grateful to Andy Layden, Nathan De Lee, and Karen Kinemuchi for useful conversations as this manuscript was being written. A.S. is grateful for support from NASA through grant AR-11277.01-A from the Space Telescope Science Institute, which is operated by the Association of Universities for Research in Astronomy, Inc., for NASA under contract NAS5-26555. The National Optical Astronomy Observatory is operated by AURA, Inc., under cooperative agreement with the National Science Foundation.

REFERENCES

- Alcock, C., et al. 2000, *AJ*, **119**, 2194
 Alonso-García, J., Mateo, M., & Worthey, G. 2004, *AJ*, **127**, 868

- Brown, T. M., et al. 2004, *AJ*, **127**, 2738
 Castellani, M., Caputo, F., & Castellani, V. 2003, *A&A*, **410**, 871
 Chaboyer, B. 1999, in *Astrophysics and Space Science Library* 237, Post-Hipparcos cosmic candles, ed. A. Heck & F. Caputo (Dordrecht: Boston), 111
 Clement, C. M. 2000, in *ASP Conf. Ser.* 203, *Impact of Large Scale Surveys on Pulsating Star Research IAU Colloq.176*, ed. L. Szabados & D. W. Kurtz (San Francisco, CA: ASP), 266
 Clementini, G., Federici, L., Corsi, C., Cacciari, C., Bellazzini, M., & Smith, H. A. 2001, *ApJ*, **559**, L109
 Contreras, R., et al. 2008, *Mem. Soc. Astron. Ital.*, **79**, 686
 Dolphin, A. E., Saha, A., Olzsewski, E., Thim, F., Skillman, E. D., Gallagher, J. J., & Hoessel, J. 2004, *AJ*, **127**, 875
 Durrell, P. R., Harris, W. E., & Pritchett, C. J. 2001, *AJ*, **121**, 2557
 Freedman, W. L., & Madore, B. F. 1990, *ApJ*, **365**, 186
 Grebel, E. K., Gallagher, J. S., III, & Harbeck, D. 2003, *AJ*, **125**, 1926
 Grillmair, C., et al. 1996, *AJ*, **112**, 1975
 Guhathakurta, P., et al. 2005, arXiv:astro-ph/0502366
 Horne, J. H., & Baliunas, S. L. 1986, *ApJ*, **302**, 757
 Irwin, M. J., Ferguson, A. M. N., Ibata, R. A., Lewis, G. F., & Tanvir, N. R. 2005, *ApJ*, **628**, L108
 Kalirai, J. S., et al. 2006, *ApJ*, **648**, 389
 Koch, A., & Grebel, E. K. 2006, *AJ*, **131**, 1405
 Koch, A., et al. 2008, *ApJ*, **689**, 958
 Layden, A. C. 1995, *AJ*, **110**, 2312
 Layden, A. C., & Sarajedini, A. 2000, *AJ*, **119**, 1760
 Mack, J., Gilliland, R. L., Anderson, J., & Sirianni, M. 2007, *ACS Instrum. Sci. Rep.* 2007–02
 Mahmud, N., & Anderson, J. 2008, *PASP*, **120**, 907
 Martin, N. F., et al. 2006, *MNRAS*, **371**, 1983
 Meylan, G., Sarajedini, A., Jablonka, P., Djorgovski, S. G., Bridges, T., & Rich, R. M. 2001, *AJ*, **122**, 830
 Mould, J., & Kristian, J. 1986, *ApJ*, **305**, 591
 Pritchett, C. J., & van den Bergh, S. 1987, *ApJ*, **316**, 517
 Reiss, A., & Mack, J. 2004, *ACS Instrum. Sci. Rep.* 2004–06
 Sandage, A. R. 1993, *AJ*, **106**, 687
 Sarajedini, A., Barker, M., Geisler, D., Harding, P., & Schommer, R. 2006, *AJ*, **132**, 1361
 Sarajedini, A., & Jablonka, P. 2005, *AJ*, **130**, 1627
 Sarajedini, A., et al. 2000, *AJ*, **120**, 2437
 Scargle, J. D. 1982, *ApJ*, **263**, 835
 Schlegel, D. J., Finkbeiner, D. P., & Davis, M. 1998, *ApJ*, **500**, 525
 Sirianni, M., et al. 2005, *PASP*, **117**, 1049
 Stetson, P. B. 1987, *PASP*, **99**, 191
 Stetson, P. B. 1994, *PASP*, **106**, 250